

NRC Publications Archive Archives des publications du CNRC

Influence of Pressure on Soot Formation in Laminar Diffusion Flames of Methane-Air up to 40 bar

Gulder, Omer L.; Thomson, Kevin A.; Weckman, Elizabeth J.; Fraser, Roydon A.; Smallwood, Gregory J.; Snelling, David R.

This publication could be one of several versions: author's original, accepted manuscript or the publisher's version. / La version de cette publication peut être l'une des suivantes : la version prépublication de l'auteur, la version acceptée du manuscrit ou la version de l'éditeur.

Publisher's version / Version de l'éditeur:

43rd AIAA Aerospace Sciences Meeting [Proceedings], 2005-1315, pp. 1-10, 2005

NRC Publications Archive Record / Notice des Archives des publications du CNRC :

<https://nrc-publications.canada.ca/eng/view/object/?id=674ddfe6-6fbd-4b38-b93d-e42c2d4c5bbc>
<https://publications-cnrc.canada.ca/fra/voir/objet/?id=674ddfe6-6fbd-4b38-b93d-e42c2d4c5bbc>

Access and use of this website and the material on it are subject to the Terms and Conditions set forth at <https://nrc-publications.canada.ca/eng/copyright>

READ THESE TERMS AND CONDITIONS CAREFULLY BEFORE USING THIS WEBSITE.

L'accès à ce site Web et l'utilisation de son contenu sont assujettis aux conditions présentées dans le site

<https://publications-cnrc.canada.ca/fra/droits>

LISEZ CES CONDITIONS ATTENTIVEMENT AVANT D'UTILISER CE SITE WEB.

Questions? Contact the NRC Publications Archive team at

PublicationsArchive-ArchivesPublications@nrc-cnrc.gc.ca. If you wish to email the authors directly, please see the first page of the publication for their contact information.

Vous avez des questions? Nous pouvons vous aider. Pour communiquer directement avec un auteur, consultez la première page de la revue dans laquelle son article a été publié afin de trouver ses coordonnées. Si vous n'arrivez pas à les repérer, communiquez avec nous à PublicationsArchive-ArchivesPublications@nrc-cnrc.gc.ca.

Influence of Pressure on Soot Formation in Laminar Diffusion Flames of Methane-Air up to 40 bar

Ömer L. Gülder*

University of Toronto, Toronto, Ontario M3H 5T6, Canada

Kevin A. Thomson,[†] Elizabeth J. Weckman[‡] and Roydon A. Fraser[§]

University of Waterloo, Waterloo, Ontario N2L 3G1, Canada

Gregory J. Smallwood[¶] and David R. Snelling^{||}

National Research Council of Canada, Ottawa, Ontario K1A 0R6, Canada

We studied laminar methane-air diffusion flames over the pressure range of 5 bar to 40 bar (0.5 MPa to 4 MPa) using a high pressure combustion chamber to investigate the effects of pressure on soot formation. The fuel flow rate was selected such that the soot was completely oxidized within the visible flame and the flame was stable at all pressures. Spectral soot emission was used to measure radially resolved soot volume fraction and soot temperature as a function of pressure. Additional soot volume fraction measurements were made using line-of-sight light attenuation. Soot concentration values from these two techniques agreed to within 30% and both methods exhibited similar trends in the spatial distribution of soot concentration. Maximum line-of-sight soot concentration depended on pressure according to a power law, where the exponent on pressure is about 1.3 for the range of pressures between 5 bar and 20 bar, and about 0.9 for 20 bar to 40 bar. Peak carbon conversion to soot, defined as the percentage of fuel's carbon content converted to soot, also followed a power-law dependence on pressure, where the pressure exponent is unity for pressures between 5 bar and 20 bar and 0.1 for 20 bar to 40 bar. The pressure dependence of sooting propensity diminished at pressures above 20 bar. Soot temperature measurements indicated that the overall temperatures decrease with increasing pressure; however, the differences diminished with increasing height in the flame. Low down in the flame, temperatures were about 150 K lower at pressures of 40 bar than those at 5 bar. In the upper half of the flame the difference in temperatures reduced to about 50 K.

I. Introduction

THE details of the chemical and physical mechanisms of soot formation process in combustion remain uncertain due to the highly complex nature of hydrocarbon flames. The mechanisms of soot formation have been investigated extensively over many years and only very broad features of the formation processes have been established. In addition to great uncertainties regarding formation mechanisms, the control and prediction of soot levels in practical combustion devices are further impeded by the complexities introduced by the transient operating conditions, existence of a two-phase turbulent flow field, and the chemistry of distillate fuels consisting of several hundred hydrocarbon compounds. One of the important parameters in soot formation is the pressure. Current understanding of the influence of pressure on soot formation and

*Professor, Institute for Aerospace Studies, 4925 Dufferin Street, Senior Member AIAA .

[†]PhD Candidate, Mechanical Engineering Department.

[‡]Associate Professor, Mechanical Engineering Department.

[§]Professor, Mechanical Engineering Department.

[¶]Group Leader, ICPET Combustion Technology, 1200 Montreal Road.

^{||}Senior Research Officer, ICPET Combustion Technology, 1200 Montreal Road.

Copyright © 2005 by authors. Published by the American Institute of Aeronautics and Astronautics, Inc. with permission.

oxidation is very sketchy, although the majority of the practical combustion devices operate at elevated pressures.

There have been a number of fundamental studies related to high pressure combustion in laminar rich premixed flat flames^{1–3}, counter-flow diffusion flames^{4–7}, and co-flow diffusion flames^{8–11}. Those related to soot formation in diffusion flames are limited to pressures lower than 10 bar. Using a diffusion flame burner operating with ethylene, Flower and Bowman⁹ report that the maximum line-of-sight integrated soot volume fractions, $f_{v_{\text{int}}}$, scale with pressure as

$$f_{v_{\text{int}}} = \int f_v(r) dr \propto P^n \quad (1)$$

where $n = 1.2 \pm 0.1$ for $P = 1$ bar to 10 bar, and $f_v(r)$ is the local soot volume fraction at radial location r . Lee and Na¹¹ also show line-of-sight integrated soot volume fractions for pressures of 1 to 4 bar in an ethylene laminar diffusion flame. Their measurements suggest $n = 1.26$. These results are difficult to interpret since they represent linearly weighted averages through an annular soot distribution, thus, neither the peak nor total soot.

The only spatially resolved measurements of soot volume fraction as a function of pressure are reported by Lee and Na¹¹. Their data are limited, but suggest

$$f_{v_{\text{max}}} \propto P^2 \quad (2)$$

for $P = 2$ to 4 bar at a height of 20 mm above the burner nozzle, where $f_{v_{\text{max}}}$ is the maximum soot volume fraction.

It is evident that information on soot in laminar diffusion flames at higher pressures is limited. In this paper we report measurements made in laminar methane-air diffusion flames over the pressures range of 5 bar to 40 bar (0.5 MPa to 4 MPa) using a high pressure combustion chamber to investigate the effects of pressure on soot formation. Spectral soot emission (SSE) was used to measure the radially resolved soot volume fraction and soot temperature as a function of pressure. Additional soot volume fraction measurements were made using the line-of-sight light attenuation (LOSA) technique. These results greatly extend any available information on flame sooting tendency as a function of pressure.

II. Experimental Methodology

The experimental high pressure combustion chamber and the laminar diffusion flame burner used in this study are described in detail in Ref.12. The design pressure of the chamber is about 100 bar (10 MPa), and its internal diameter and internal height are 0.24 m and 0.6 m, respectively. Optical access into the chamber is through three ports at 0, 90, and 180 degree locations allowing line-of-sight measurements as well as 90° scattering and imaging experiments. A schematic of the chamber is shown in Fig.1. The laminar diffusion flame burner used in this work was built based on a design by Miller and Maahs⁸ who achieved a stable flame over a pressure range of 1 bar to 50 bar by placing a circular quartz chimney around the flame. The burner has a fuel nozzle exit diameter of 3.06 mm and an air nozzle diameter of 25 mm. Sintered metal foam elements (80 pores per inch) are included in the fuel and air nozzles to straighten and reduce instabilities in the flow and to create a top hat exit velocity profile as the gases leave the foam elements. A tapered fuel nozzle reduces recirculation from the burner tip and improves stability of the fluid-ambient interface⁸. In the original design, a cylindrical quartz tube surrounded the flame to aid flame stabilization. For the present experiments, the quartz tube was replaced by a new chimney designed to include three flat windows aligned with the three

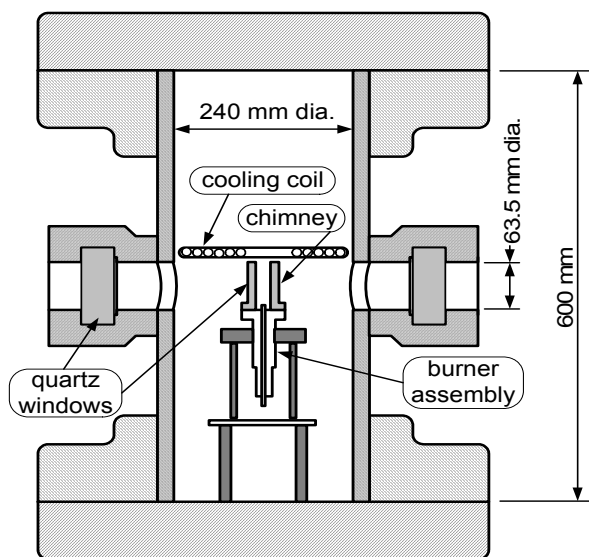


Figure 1. A schematic of the high pressure combustion chamber with a design pressure of 100 bar.

viewing ports on the chamber. The flame is ignited using a glow plug incorporated into the chimney and located above the flame.

Flame stability was assessed at pressures of 5, 10, 20, and 40 bar using a digital video camera for methane flow rates of 0.55 and 0.66 mg/s, and air flow rate of 0.4 g/s. Flames exhibited good, long term stability for all pressures with an *rms* flicker of the flame tip less than 0.1 mm. Representative still images of methane-air laminar diffusion flames at pressures from 1 bar (0.1 MPa) to 80 bar (8 MPa) are shown in Fig.2.

The theory and overall experimental layout of the spectral soot emission diagnostic (SSE) are described previously¹³. In SSE, line-of-sight radiation emission from soot is measured along chords through the flame. A series of emission projections at a given height in the flame can be inverted to obtain radially resolved emission rates from which temperature and soot volume fraction can be determined when soot optical properties are known. For the current measurements a 300 mm focal length lens (f/45, 2:1 magnification) is used to image the object plane at burner centre onto a vertical entrance slit (height 0.500 mm, width 0.025 mm) of a spectrometer. Output from the spectrometer is imaged onto a 16-bit CCD detector (1100 pixels×330 pixels). Knife edge scans across a diffuse light source located at the object plane show a horizontal spatial resolution of 50 μm. The system is calibrated for radiation intensity using a calibrated filament lamp placed inside the chamber. The uncertainty in the spectral radiance temperature is 5 K. Soot emission is measured over a wavelength range of 690-945 nm. Spectra are averaged over the vertical height of the entrance slit as well as across 21 nm spectral widths, thus providing 12 spectral data points per line-of-sight acquisition. One-dimensional tomography is applied to each wavelength range using a three-point Abel inversion method¹⁴. Local temperatures are determined from the spectral shape of the inverted soot emission intensity. Soot volume fraction is then determined from the soot emission intensity using the measured temperatures. The soot refractive index function, $E(m)$, is assumed to be constant and equal to 0.274 for the calculations. This assumption is consistent with results of Krishnan et al.¹⁵. Sensitivity of SSE results to $E(m)$ is discussed in Ref.13. Modelling of the flame emission using the methods described in Ref.13 shows that emission attenuation by soot introduces only a small error (i.e. < 2%) in the measurements for even the highest soot loadings observed in this flame. Therefore no attenuation correction is applied.

The line-of-sight attenuation (LOSA) diagnostic is a simplified version of the 2D LOSA diagnostic described in Ref.16. In LOSA, line-of-sight measurement of the intensity of small light beam transmitted through a flame is made. When divided by a measurement of the intensity of the beam transmitted along the same path without the flame present, the transmissivity of the flame along the chord can be determined. A series of transmissivity measurements at a given height in the flame can be inverted to obtain radially resolved extinction coefficients from which soot volume fraction can be determined. The optical layout for the LOSA measurements is included in Fig.3. Light from a mercury arc lamp is first focussed onto a 50 μm pinhole. Light transmitted through the pinhole is modulated using a chopper wheel and imaged at the centre plane of the burner with a 1.5:1 demagnification at a speed of f/19. Knife edge scans of the lamp beam at burner centre show the beam width to be less than 40 μm across the diameter of the burner nozzle. A collection lens downstream of the burner re-focuses the transmitted

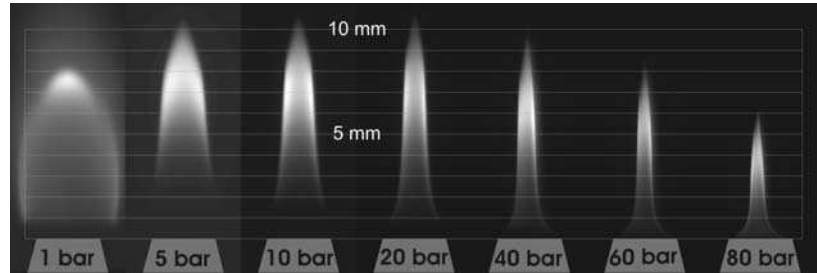


Figure 2. Images of methane-air laminar diffusion flames at pressures from 1 bar (0.1 MPa) to 80 bar (8 MPa). At all pressures the methane and total air flow rates were kept constant at 0.66 mg/s and 0.4 g/s, respectively.

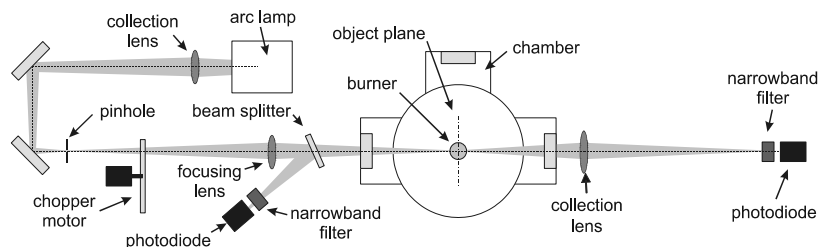


Figure 3. Schematic of the line-of-sight (LOSA) diagnostic.

light. A series of transmissivity measurements at a given height in the flame can be inverted to obtain radially resolved extinction coefficients from which soot volume fraction can be determined. The optical layout for the LOSA measurements is included in Fig.3. Light from a mercury arc lamp is first focussed onto a 50 μm pinhole. Light transmitted through the pinhole is modulated using a chopper wheel and imaged at the centre plane of the burner with a 1.5:1 demagnification at a speed of f/19. Knife edge scans of the lamp beam at burner centre show the beam width to be less than 40 μm across the diameter of the burner nozzle. A collection lens downstream of the burner re-focuses the transmitted

lamp light onto a photodiode detector coupled to a lock-in amplifier. The collection lens is large (i.e., 100 mm dia.) to accommodate beam steering of the light transmitted through the flame, which becomes quite pronounced at 40 bar. A glass plate located between the imaging lens and chamber reflects a portion of the lamp light onto a second photodiode which is used to ratio out temporal variation in the lamp intensity. Both photodiodes are filtered with 830 nm narrow band filters. For each measurement height, two scans are required, one with the flame lit and the second with the flame extinguished. The method used to calculate soot volume fraction measurements from line-of-sight transmissivity measurements is described in Ref.16.

Measurements of soot volume fraction and temperature were obtained using SSE and LOSA for pressures of 5, 10, 20, and 40 bar. A constant mass flow rate of methane and air of 0.55 mg/s and 0.4 g/s, respectively, was maintained across all pressure. For each pressure, measurements were obtained at height increments of 0.5 mm from the base to the tip of the flame and at horizontal increments of 50 μm .

III. Results and Discussion

The shape of the flame changed considerably with pressure, Fig. 3. At atmospheric pressure, the flame had a bulbous appearance and, at its widest point, was wider than the burner nozzle exit diameter. Soot was present only at the tip of the flame. As pressure increased, the visible luminosity dramatically increased, the soot zone extended down to the tip of the burner, and the flame narrowed. At all pressures above atmospheric, gas emissions were not visible, being swamped by the much stronger soot emissions. Flame height increased gradually from 5 to 20 bar and then decreased with further increases in pressure. These trends are consistent with observations by Miller and Maahs⁸ for a 0.46 mg/s methane flame, however, the peak flame height was observed at 10 bar for their flames in contrast to 20 bar in the present work. This might be due to the small differences in fuel mass flow rate used in the two studies.

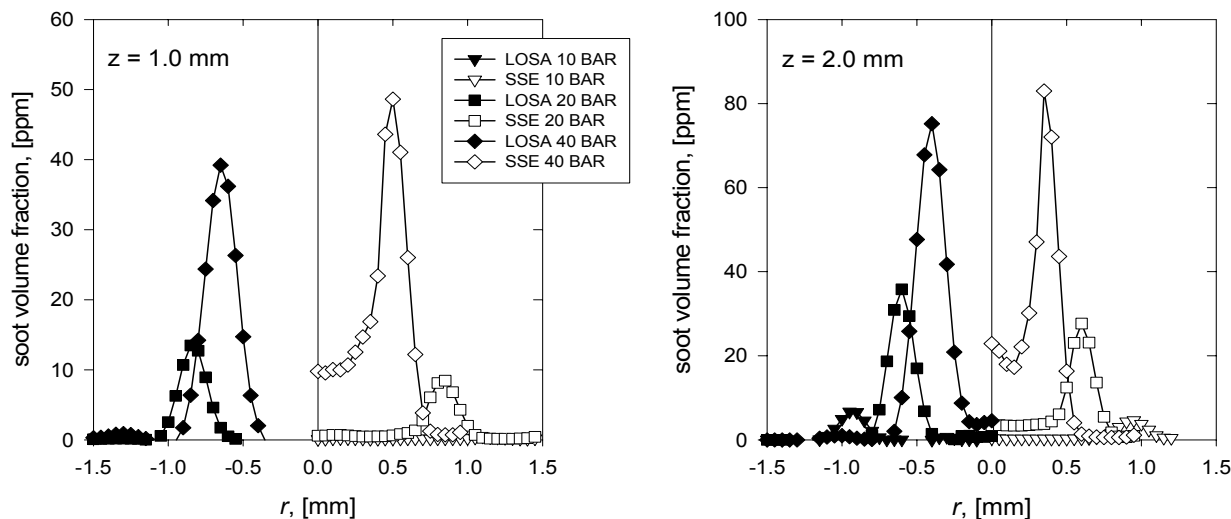


Figure 4. Radial soot concentration profiles at heights of 1 mm and 2 mm at 10, 20, and 40 bar (1, 2, and 4 MPa) pressures. LOSA measurements are shown on left panels, full symbols, and SSE measurements are on the right panels, open symbols.

To allow comparison of results for different pressures, it is important to maintain similar reference conditions. To achieve this a constant mass flow rate of fuel was maintained at all pressures, thus allowing a constant carbon release from the nozzle based on the fuels chemical composition. Similarly, it is desirable to view the progression of the soot formation and destruction at similar residence times. Theoretical analysis suggests that the height of a constant mass flow rate diffusion flame is invariant with pressure¹⁷. This prediction is approximately true over the pressure range studied.

Profile of soot volume fraction measurements for heights of $z = 1.0$ to 8.0 mm are shown in Figs.4-7. SSE and LOSA measurements are presented in the same figures to allow direct comparison of the results. For both methods, scans across the entire flame diameter were performed; however, only the average of the data from the left and right side scans are presented in the figures.

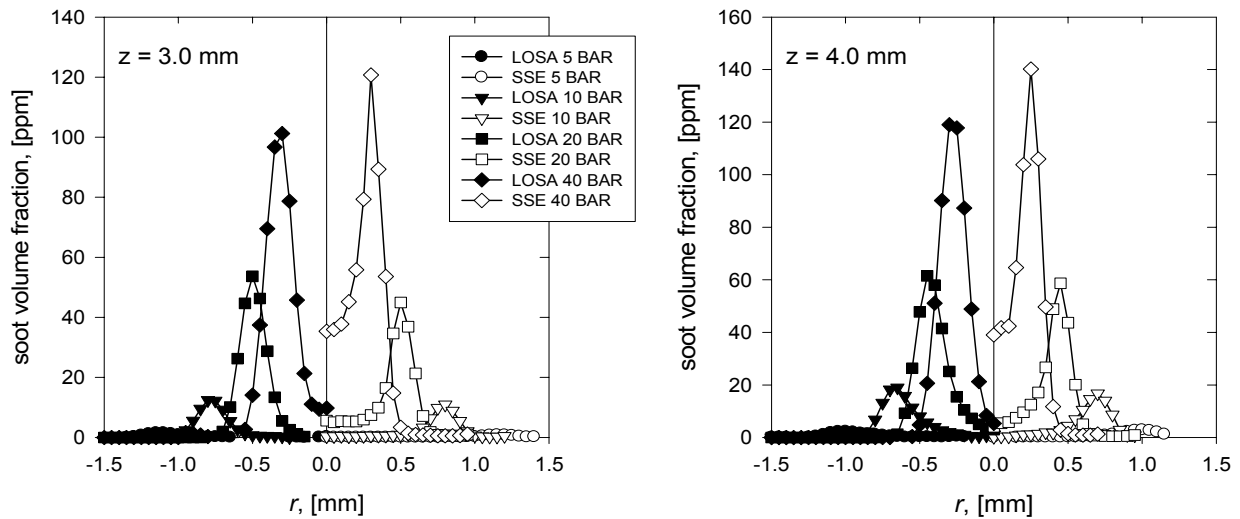


Figure 5. Radial soot concentration profiles at height of 3 mm and 4 mm at 5, 10, 20, and 40 bar (0.5, 1, 2, and 4 MPa) pressures. LOSA measurements are shown on left panels, full symbols, and SSE measurements are on the right panels, open symbols.

Much like the commonly used atmospheric pressure burners^{13,18}, the soot formed first in an annular band near the burner rim. Near the mid height of the flame, the annular distribution of soot remained pronounced, but soot also began to appear in the core of the flame. At the tip of the flame, the annular distribution disappeared and a peak soot concentration was observed on the flame centreline. From the curves in Figs. 4 to 7, the significant contraction of the flame diameter with pressure is reflected in the location of the peaks in the radial profiles of soot volume fraction. Additionally, a steep increase of soot concentration with pressure is noted in the soot concentration curves.

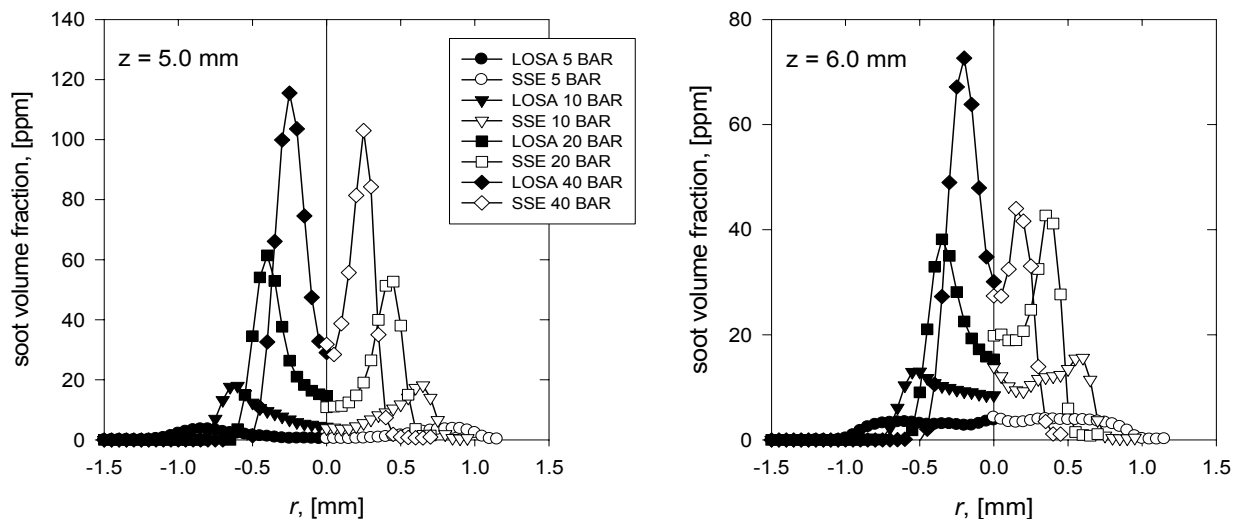


Figure 6. Radial soot concentration profiles at height of 5 mm and 6 mm at 5, 10, 20, and 40 bar (0.5, 1, 2, and 4 MPa) pressures. LOSA measurements are shown on left panels, full symbols, and SSE measurements are on the right panels, open symbols.

The agreement in trends and distributions of soot volume fraction as measured by SSE and LOSA is satisfactory. The curves have very similar shape and locations of the peak soot concentrations correspond to within 10%. The SSE curves often suggest higher values of soot concentration in the core of the flame. This may relate to the problems with background radiation entering the line-of-sight measurements¹². For

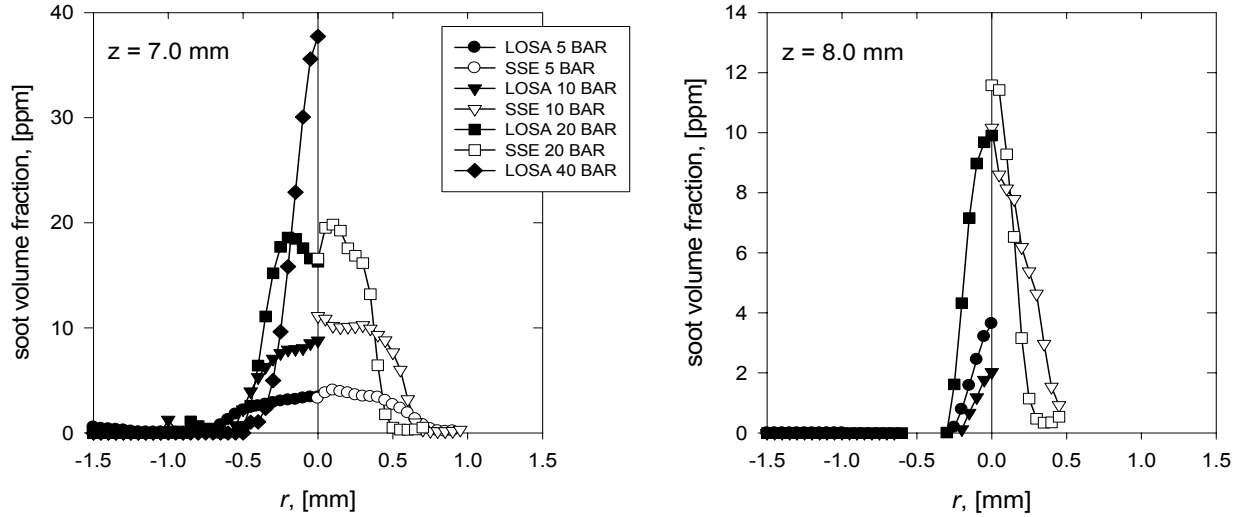


Figure 7. Radial soot concentration profiles at height of 7 mm and 8 mm at 5, 10, 20, and 40 bar (0.5, 1, 2, and 4 MPa) pressures. LOSA measurements are shown on left panels, full symbols, and SSE measurements are on the right panels, open symbols.

pressures of 5 to 20 bar, the LOSA results typically indicate higher values of soot volume fraction than the SSE results. It is possible that ratio of light scatter to absorption was underestimated in the calculations, which would lead to higher LOSA derived values of soot volume fraction. At $P = 40$ bar, the SSE soot volume fraction measurements suggest higher concentrations than the LOSA measurements up to $z = 4.0$ mm, beyond which the SSE measurements are lower than the LOSA measurement. At $z = 7.0$ and 8.0 mm, the agreement between the measurements is less consistent. It is possible that flame flicker is more pronounced at these heights at this high pressure. Though there are some exceptions (e.g., $P = 10$ bar, $z = 8.0$ mm), for the most part the two diagnostics generally agree to within 30%.

It is expected that soot volume fractions would increase with increasing pressure since the flame is narrowing so that all species are in higher concentration. To quantify the sooting propensity of the flame at different pressures it is useful to calculate the percentage of total carbon converted to soot as a function of height. The mass flow rate of carbon, in the form of soot, can be determined through the relationship:

$$\dot{m}_s = v_z(z)\rho_s \int 2\pi r f_v(r, z) dr \quad (3)$$

where v_z is the axial velocity and $\rho_s = 1.8$ g/mL is the soot density. The axial velocity is estimated using the relationship $v_z(z) = \sqrt{2az}$, where a is an acceleration constant commonly assumed^{9,19} to be 25 m/s². The percentage of carbon in the fuel converted to soot is simply $f_s = \dot{m}_s/\dot{m}_c$, where \dot{m}_c is the carbon mass flow rate at the nozzle exit. Peak carbon conversion occurs at a height of about 5.5 mm above the burner nozzle for pressures of 5 and 10 bar, 5.0 mm for a pressure of 20 bar, and 4.0 mm for a pressure of 40 bar, Fig.8. Up to the point of peak carbon conversion, the curves are approximately linear with height and their slope increase with pressure. Peak carbon conversion scales with pressure as $f_s \propto P^n$, where $n = 1$ for the pressure range of 5 to 20 bar and $n = 0.1$ for the pressure range of 20 to 40 bar, Fig.9. Thus, it is shown that soot formation is

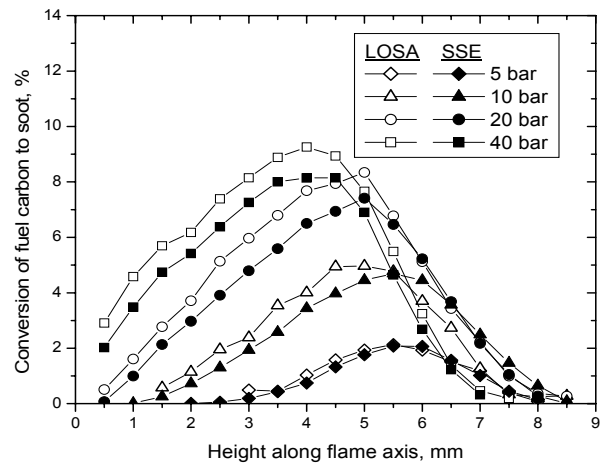


Figure 8. Percent conversion of carbon to soot as a function of axial location.

enhanced by pressure even when density effects are removed. However, at pressures between 20 and 40 bar, the sensitivity is quite low and it is speculated that the maximum carbon conversion to soot could begin to drop at pressures above 40 bar. Further measurements about 40 bar are needed to understand better the sooting trends at these higher pressures. It is noted that carbon conversion to soot in this methane flame peaks at a value of about 9%, Fig.9, compared to 40-50% observed by Flower and Bowman in an ethylene flame⁹.

To compare the current results with those of Flower and Bowman⁹ and Lee and Na¹¹, line integrals of the soot concentration profiles were calculated. It is found that the maximum line integrated soot volume fraction, $f_{v, \text{int}}$, varies as $f_{v, \text{int}} \propto P^n$, where $n = 1.3$ for $P = 5$ to 20 bar and $n = 0.9$ for $P = 20$ to 40 bar. It is noted that for the lower pressure range, the correlation agrees with results of Flower and Bowman⁹ and Lee and Na¹¹ and that the agreement with the carbon conversion rate is fair; however, for the 20 and 40 bar pressure range, the peak line-of-sight integrated soot volume fraction pressure correlation does not show the step reduction in the soot production rate which is captured by the peak soot conversion pressure correlation. It is therefore concluded that line-of-sight integrated soot volume fraction can be a misleading measure of sooting tendency at elevated pressures.

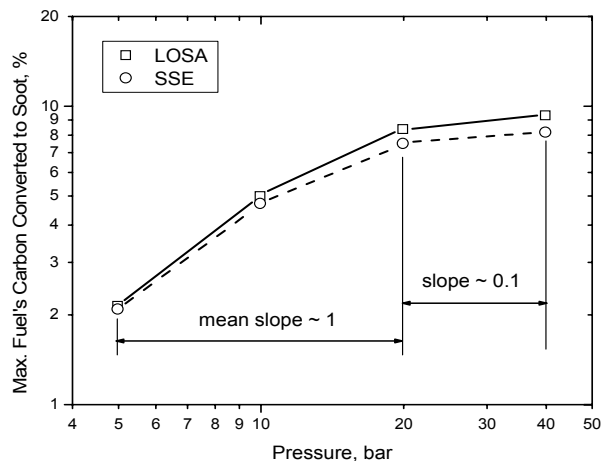


Figure 9. Maximum percent conversion of carbon from fuel to soot as a function of pressure.

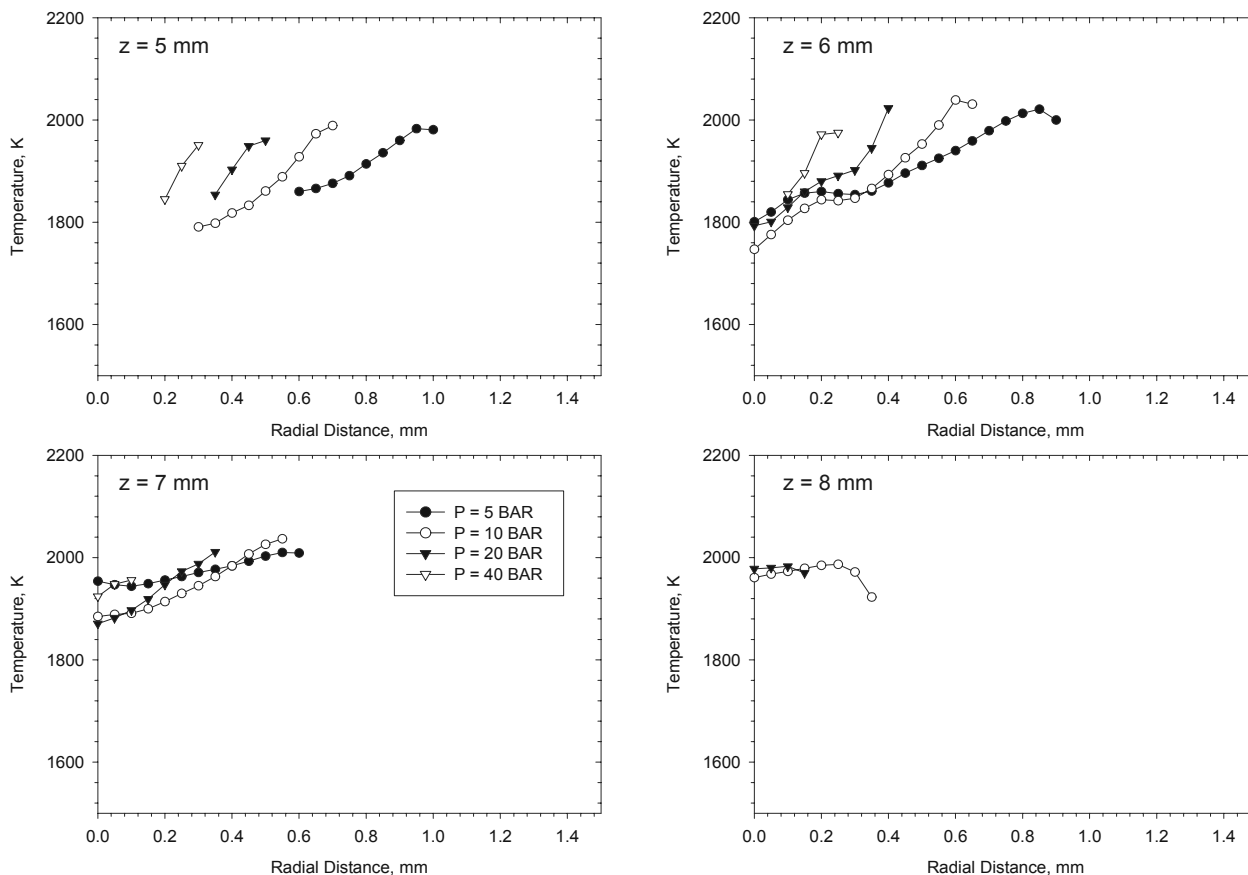


Figure 10. Radial soot temperature profiles at heights of 5 to 8 mm at 5, 10, 20, and 40 bar (0.5, 1, 2, and 4 MPa) pressures.

Measured soot temperatures for pressures of 5, 10, 20, and 40 bar are shown in Fig.10. Since the measurements are based on measurements of soot emission, temperatures can only be determined in locations where sufficient soot exists to provide a resolvable signal. This typically occurs at radial locations centred about the zones of peak soot volume fraction. From previous characterization of the SSE diagnostic¹³, temperatures are known to decrease at the outer edges of the annuli earlier than would be predicted by flame models or other experimental diagnostics, thus under-predicting the peak temperature in the reaction zone. It is believed that this fall off is caused by errors introduced through the inversion algorithm when inverting the rapidly decreasing line-of-sight emission intensities at the edge of the flame. In the core of the flame, temperatures can also be inaccurate when soot volume fractions are low relative to peak soot volume fractions in the annulus. Consequently, the temperature plots provided here have been limited to regions centered about the soot annuli. This is justified by the fact that the agreement between soot volume fraction measurements using SSE and LOSA in these regions is good and requires an accurate estimation of the soot temperature. The radial temperature profiles are qualitatively similar to those observed in atmospheric pressure diffusion flames^{13,19}.

To allow a more consistent comparison with the results of Flower¹⁰, temperatures were calculated from line-of-sight emission measurements through the flame centre, Fig. 11. Since the measurements are line-of-sight, they represent a soot concentration weighted average temperature along a chord through the flame and should correspond closely to the peak soot volume fraction temperatures. The results are similar to those of Flower¹⁰ in that a high temperature region is observed near the base of the flame. This high temperature region likely exists because of preheating of reactants from the nozzle and from the flame reaction zone which resides concentrically outside of the soot annulus. The temperature minima move towards the burner outlet with increasing pressure. This correlates well with the carbon conversion to soot which begins closer to the tip of the burner with increasing pressure. Additionally, temperature increases with height from a minimum value near the burner outlet. The rate of increase

increases with pressure. The range of observed temperatures (i.e., the range from the minimum to maximum temperatures) increases with pressure from $\Delta T = 100$ K at $P = 5$ bar to $\Delta T = 250$ K at $P = 40$ bar. Average temperatures drop with increasing pressure, though the effect is less pronounced in the upper half of the flame. In flames reported by Flower¹⁰, the average soot particle temperature of line-of-sight measurements through the flame centre decreases with height in the upper half of the flame except at a pressure of 1 bar. The reason for this behaviour is that all flames, except that at 1 bar, were soot emitting (i.e., smoking) flames, therefore soot is not completely oxidized and it escapes from the flame tip. In flames studied in the present work no soot escapes from the flame tip, therefore all soot is oxidized within the visible yellow/orange flame region. For this reason, the average temperatures shown in Fig.11 display an increase with downstream distance along the flame axis. The temperature curves converge at the tip of the flame in the current study. This was not observed in the flames of Flower¹⁰ due to the cessation of soot oxidation.

Temperatures in Fig. 11 show a definite and significant decrease with increasing pressure at axial locations up to 4-5 mm. At locations higher than 4-5 mm, soot concentrations start decreasing rapidly due to soot oxidation, Fig.8. The heat release resulting from oxidation of soot at higher pressures keeps local temperatures close to the temperatures seen in lower pressure cases, as shown in Fig.11. Also, the local radiation heat loss is less pronounced due to lower soot concentrations (as well as lower temperatures). Finally, radial temperature gradients are reduced as the core of the flame has been heated by the soot annulus. The interplay of these phenomena seems to determine the temperature trends observed in Fig. 11. This explanation also resolves the question of how, in spite of the mild temperature increases expected with increasing pressure, observed soot temperatures were lower at higher pressures.

Reliable measurements with the SSE method were only possible in the radial region around the peak local

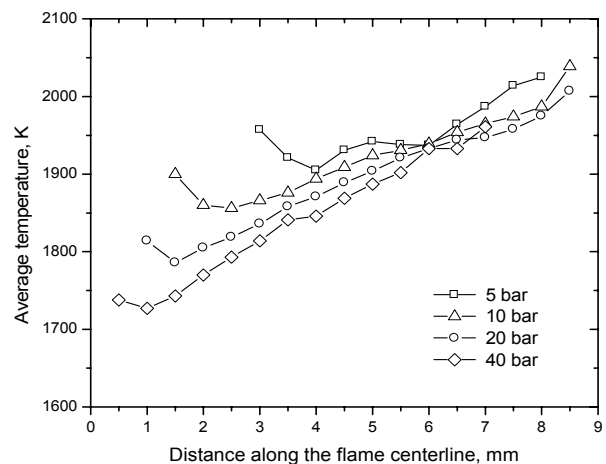


Figure 11. Line-of-sight emission averaged soot temperature as a function of axial location.

emission intensity annulus. The total uncertainty of the temperature and soot volume fraction measurements is dominated by the uncertainty of the soot refractive index. The total uncertainty in temperature is 3.5% and the total uncertainty in soot volume fraction is 40% with a 95% confidence interval. Total uncertainty of the soot volume measurements of with the LOSA method was 20-30% with a 95% confidence interval.

IV. Conclusions

The work presented here represents a significant contribution to the understanding of the impact of pressure on soot formation. A stable and reliable flame has been demonstrated and used to collect spatially resolved measurements of soot volume fraction and temperature in laminar co-flow diffusion flames over the pressure range of 5 to 40 bar (0.5 to 4.0 MPa) . Such measurements have not been achieved previously.

Peak carbon conversion to soot mass increases with pressure as $f_s \propto P^n$, where $n = 1$ for $P = 5$ to 20 bar and $n = 0.1$ for $P = 20$ to 40 bar. It is apparent from these correlations that soot formation is enhanced by pressure but that it becomes less sensitive to pressure above 20 bar. The plots of f_s versus axial distance along the flame centerline show that the start of significant soot formation moves closer to the burner nozzle with increasing pressure. This supports the observations of Heidermann et al.³ that fuel pyrolysis and soot nucleation are enhanced by pressure. The soot measurements, when appropriately transformed, are also consistent with the line-averaged measurements of Flower and Bowman⁹ and Lee and Na¹¹. However, line-averaged soot volume fraction measurements do not provide a clear picture of the trends of soot formation as a function of pressure.

Acknowledgments

This work was performed at the National Research Council of Canada and supported in part by the AFTER POL of the Canadian Government's PERD program. Funding for K. A. Thomson has been provided in part by a Carl A. Pollock Fellowship from the University of Waterloo, research grants from the Natural Sciences and Engineering Research Council (NSERC) of Canada, as well as a Graduate Student Supplement Scholarship from the National Research Council of Canada.

References

- ¹Böhm, H., Feldermann, C., Heidermann, T., Jander, H., Luers, B., and Wagner, H. G., "Soot Formation in Premixed C₂H₄-Air Flames for Pressures up to 100 bar", *Proceedings of the Combustion Institute*, Vol. 24, 1992, pp. 991-998.
- ²Hanisch, S., Jander, H., Pape, T., and Wagner, H. G., "Mass Growth and Coagulation of Soot Particles in C₂H₄/Air-Flames at 15 bar", *Proceedings of the Combustion Institute*, Vol. 25, 1994, pp. 577-584.
- ³Heidermann, T., Jander, and Wagner, H. G., "Soot Particles in Premixed C₂H₄-Air Flames at High Pressures (P=30-70 bar)", *Physical Chemistry Chemical Physics*, Vol. 1, No.15, 1999, pp.3497-3502.
- ⁴Ravikrishna, R. V., Thomsen, D. D., and Laurendeau, N. M., "Laser-Induced Fluorescence Measurements and Modeling of Nitric Oxide in High-Pressure Counterflow Diffusion Flames", *Combustion Science and Technology*, Vol.157, 2000, pp. 243-261.
- ⁵Fotache, C. G., Kreutz, T. G., and Law, C. K., "Ignition of Hydrogen-Enriched Methane by Heated Air", *Combustion and Flame*, Vol.110, No.4, 1997, pp.429-440.
- ⁶Saur, A. M., Behrendt, F., and Franck, E. U., "Calculation of High Pressure Counterflow Diffusion Flames up to 3000 bar", *Berichte der Bunsen-Gesellschaft für Physikalische Chemie*, Vol.97, No.7, 1993, pp.900-908.
- ⁷Sohn, C. H., and Chung, S. H., "Effect of Pressure on the Extinction, Acoustic Pressure Response, and NO Formation in Diluted Hydrogen-Air Diffusion Flames", *Combustion and Flame*, Vol.121, No.1-2, 2000, pp.288-300.
- ⁸Miller, I. M., and Maahs, H. G., "High-Pressure Flame System for Pollution Studies with Results for Methane-Air Diffusion Flames", NASA Technical Paper TN D-8407, 1977.
- ⁹Flower, W. L., and Bowman, C. T., "Measurements of the Structure of Sooting Laminar Diffusion Flames at Elevated Pressures", *Proceedings of the Combustion Institute*, Vol. 21, 1986, pp.1115-1124.
- ¹⁰Flower, W. L., "Soot Particle Temperatures in Axisymmetric Laminar Ethylene-Air Diffusion Flames at Pressures up to 0.7 MPa", *Combustion and Flame*, Vol.77, 1989, pp.279-293.
- ¹¹Lee, L., and Na, Y. D., "Soot Study in Laminar Diffusion Flames at Elevated Pressure Using Two-Color Pyrometry and Abel Inversion", *JSME International Journal Series B*, Vol. 43, No. 4, 2000, pp. 550-555.
- ¹²Thomson, K. A., "Soot Formation in Annular Non-premixed Laminar Flames of Methane-Air at Pressures of 0.1 to 4.0 MPa", Ph.D. Dissertation, Mechanical Engineering Department, University of Waterloo, Ontario, 2005.

- ¹³Snelling, D.R., Thomson, K.A., Smallwood, G.J., Gülder, Ö. L., Weckman, E. J., and Fraser, R. A., "Spectrally Resolved Measurement of Flame Radiation to Determine Soot Temperature and Concentration", *AIAA Journal*, Vol. 40, No. 9, 2002, pp.1789-1795.
- ¹⁴Dasch, C. J., "One-Dimensional Tomography: A Comparison of Abel, Onion-Peeling, and Filtered Backprojection Methods.", *Applied Optics*, Vol. 31, No. 8, 1992, pp. 1146-1152.
- ¹⁵Krishnan, S. S., Lin, K. -C., and Faeth, G. M., "Optical Properties in the Visible of Overfire Soot in Large Bouyant Turbulent Diffusion Flames", *Journal of Heat Transfer*, Vol. 122, 2000, pp. 517-524.
- ¹⁶Snelling, D. R., Thomson, K. A., Smallwood, G. J., and Gülder, Ö. L., "Two-Dimensional Imaging of Soot Volume Fraction in Laminar Diffusion Flames", *Applied Optics*, Vol. 38, No. 12, 1999, pp. 2478-2485.
- ¹⁷Roper, F. G., "The Prediction of Laminar Jet Diffusion Flame Sizes. I. Theoretical Model", *Combustion and Flame*, Vol. 29, No. 3, 1977, pp. 219-226.
- ¹⁸Santoro, R. J., and Semerjian, H. G., "Soot Formation in Diffusion Flames: Flow Rate, Fuel Species, and Temperature Effects", *Proceedings of the Combustion Institute*, Vol.20, 1984, pp. 997-1006.
- ¹⁹Santoro, R. J., Yeh, T. T., Horvath, J. J., and Semerjian, H. G., "The Transport and Growth of Soot Particles in Laminar Diffusion Flames", *Combustion Science and Technology*, Vol. 53, No. 2-3, 1987, pp. 89-115.